Grain boundary-induced variability of charge transport in hydrogenated polycrystalline graphene

Barrios-Vargas, Jose E.; Falkenberg, Jesper Toft; Soriano, David; Cummings, Aron W.; Brandbyge, Mads; Roche, Stephan

Published in:
2D materials

Link to article, DOI:
10.1088/2053-1583/aa59de

Publication date:
2017

Document Version
Peer reviewed version

Grain boundary-induced variability of charge transport in hydrogenated polycrystalline graphene

Jose E. Barrios Vargas,[*,†,§] Jesper T. Falkenberg,[‡,§] David Soriano,[†] Aron W. Cummings,[†] Mads Brandbyge,[‡] and Stephan Roche[*,†,¶]

†*Catalan Institute of Nanoscience and Nanotechnology (ICN2), CSIC and The Barcelona Institute of Science and Technology, Campus UAB, 08193 Barcelona, Spain*
‡*Department of Micro- and Nanotechnology (DTU Nanotech), Center for Nanostructured Graphene (CNG), Technical University of Denmark, DK-2800 Kgs. Lyngby, Denmark*
¶*ICREA - Institució Catalana de Recerca i Estudis Avançats, 08010 Barcelona, Spain*
§*These authors contributed equally to this work.*

E-mail: jose.barrios@icn2.cat; stephan.roche@icn2.cat

Abstract

Chemical functionalization has proven to be a promising means of tailoring the unique properties of graphene. For example, hydrogenation can yield a variety of interesting effects, including a metal-insulator transition or the formation of localized magnetic moments. Meanwhile, graphene grown by chemical vapor deposition is the most suitable for large-scale production, but the resulting material tends to be polycrystalline. Up to now there has been relatively little focus on how chemical functionalization, and hydrogenation in particular, impacts the properties of polycrystalline graphene. In this work, we use numerical simulations to study the electrical properties of hydrogenated polycrystalline graphene. We find a strong correlation between the spatial distribution of the hydrogen adsorbates and the charge transport properties. When the hydrogen is confined to the grain boundaries there is little impact on charge transport, while a uniform distribution of hydrogen yields a significant degradation of the electronic mobility. This difference is related to the resonant impurity states induced by the hydrogen adsorbates; these states can form when the hydrogen is in the pristine graphene grains, but not when the hydrogen is within the grain boundary. These results suggest that one can tune the electrical transport of polycrystalline graphene through selective hydrogen functionalization, and they also have important implications for hydrogen-induced magnetization and spin lifetime of this material.

Introduction

Since its experimental isolation in 2004[1], single-layer graphene has emerged as an exciting material for a wide variety of applications. Much of this excitement stems from graphene's remarkable electrical[1], optical[2], thermal[3], and mechanical properties[4]. In addition to its unique intrinsic properties, another promising characteristic of graphene is its tunability. In particular, because graphene is two-dimensional, chemical functionalization has been studied as an effective approach to extrinsically tune its material properties. For example, metallic adatoms can potentially induce a strong spin-orbit coupling in graphene[5] and oxygen adsorption can significantly alter graphene's thermo-

electric characteristics[6]. An adsorbate of particular interest is hydrogen, which forms a covalent bond to a single carbon atom and induces a resonant impurity state around the graphene Dirac point[7,8]. This can have a considerable impact on electronic transport, as revealed by measurements of a metal-insulator transition with increasing hydrogen density[9]. Recent experimental work has also shown that hydrogen induces a localized magnetic resonance[10], which could have important implications for graphene spintronics[11,12].

While mechanical exfoliation tends to yield the highest-quality graphene samples in the laboratory, chemical vapor deposition (CVD) is the most efficient method to produce graphene on an industrial scale. This method is now capable of producing single graphene grains reaching the centimeter scale[13–15], but faster CVD growth yields much smaller grains, resulting in a material that is polycrystalline[15]. In polycrystalline graphene, the grain boundaries (GBs) between misoriented grains consist of a series of non-hexagonal rings[16–18] that can impede charge transport through the material[19–21]. In addition, GBs tend to be more chemically reactive than pristine graphene, which can also strongly impact charge transport, making this material interesting for gas sensing applications[22,23]. Prior studies have examined the impact of hydrogenation on the electronic transport properties of polycrystalline graphene[9,24], but the detailed nature of the interaction between GBs and hydrogen adsorbates remains unclear.

In this work, we use *ab initio* and tight-binding (TB) calculations to study the impact of hydrogenation on the electronic properties of polycrystalline graphene. We find that the precise distribution of hydrogen adatoms is crucial for predicting their effect. Specifically, when the hydrogenation is confined to the GBs, the overall impact on charge transport is negligible, which is in sharp contrast to the case of hydrogenation within the grains. We find that this difference is related to the formation (or not) of the resonant impurity state near the Dirac point; hydrogen adsorbates induce resonant states within the graphene grains but not in the GBs. These results suggest the possibility of tuning the electrical transport of polycrystalline graphene through selective hydrogen functionalization, and also have important implications for hydrogen-induced magnetic transport properties.

Hydrogenation of a Stone-Wales defect

We begin our study with a canonical structural defect in graphene, the Stone-Wales (SW) defect. As shown in Figures 1(a) and (b), a SW defect consists of a 90-degree rotation of a single carbon-carbon bond, turning four hexagons into two pairs of pentagons and heptagons. In this defect, and in GB structures in general, we classify "interior" defect sites as the carbon sites that only belong to non-hexagonal rings, and "exterior" defect sites as those that belong to both hexagonal and non-hexagonal rings. By this definition, the exterior sites lie on the boundary between the SW defect (or the GB) and the pristine graphene region. Various *ab initio* calculations have shown that the interior sites are more favorable for chemical adsorption[25,26]. To study the impact of hydrogenation, we calculated the electronic band structure of the SW defect with a single hydrogen impurity at either an interior or an exterior defect site, as shown schematically in Figures 1(a) and (b). The calculations were performed using the SIESTA *ab initio* package[27] using the PBE-GGA density functional[28] including full structural relaxation of a 7x7 unit cell using a 8×8 k-point sampling, and employing a double-zeta polarized basis set. The resulting band structures are shown in Figures 2(a) and (b), and indicate a clear difference between the two cases. As seen in Figure 2(b), hydrogenation of an exterior site opens a band gap and induces a strongly localized impurity state around the Fermi energy, similar to what is seen in hydrogenated pristine graphene[7,8]. In constrast, Figure 2(a) shows that the localized impurity state is completely suppressed when hydrogenating the interior defect site. How does this compare to the band structure of the SW defect with-

out hydrogen? I tried to look briefly at the band structure and shift the Fermi-level to add an electron but could not make sense of it, so more time is needed here.. maybe we can leave it for now(?)

These results echo those reported by other groups[29,30], and they speak to the importance of the local atomic structure in determining the formation of localized impurity states. According to graph theory, the number of zero-energy eigenvalues in a bipartite lattice is given by $n_0 = |n_A - n_B|$, where n_A and n_B are the number of sites in each sublattice[31]. At all carbon sites around the SW defect, the bipartite nature of the graphene lattice is preserved and hydrogenation will induce an impurity state at zero energy (the Dirac point). However, the two interior atoms of the SW defect are each connected to both sublattices of the surrounding bipartite lattice, and thus they cannot be assigned to either of the two sublattices. In this case, hydrogenation does not induce an imbalance of the two sublattices, and the zero-energy impurity state does not form.

Hydrogenation of polycrystalline graphene

Moving beyond the SW defect, we now consider hydrogenation of a more realistic polycrystalline graphene sample. For this work, a large-area polycrystalline sample containing ~2.2 million atoms was generated according to the method of Ref.[32], with an average grain diameter of 21 nm. Owing to its size, the electronic properties of this sample were described by a nearest-neighbor tight-binding (TB) model with a single p_z-orbital per carbon site. As shown by the dashed lines in Figure 2, this simple model does a good job of reproducing the *ab initio* calculations of the SW defect. To calculate electronic tranport in the polycrystalline sample, we employed a real-space order-N wave packet propagation method[33,34]. Through this method one can calculate the time-dependent diffusion coefficient as

$$D(E,t) = \frac{\partial}{\partial t}\Delta X^2(E,t), \tag{1}$$

where ΔX^2 is the mean-square displacement of the wave packet,

$$\Delta X^2(E,t) = \frac{\mathrm{Tr}[\delta(E-\hat{H})|\hat{X}(t)-\hat{X}(0)|^2]}{\rho(E)}, \tag{2}$$

and $\rho(E) = \mathrm{Tr}[\delta(E-\hat{H})]$ is the density of states (DOS), which we calculated using a kernel polynomial method. Finally, the semiclassical conductivity, mean free path, and mobility were calculated as $\sigma(E) = e^2\rho(E)D_{max}(E)$, $\ell_e(E) = D_{max}(E)/2v_F(E)$, and $\mu(E) = \sigma(E)/n(E)$, where D_{max} is the maximum value of the time-dependent diffusion coefficient, v_F is the electron Fermi velocity, and n is the charge density, obtained by integrating the DOS.

In our transport calculations, we considered three distributions of hydrogen adsorbates. Similar to the SW defect, we considered hydrogenation of only the interior and exterior GB sites, and also a random distribution of hydrogen throughout the entire sample. These distributions are shown schematically in Figures 1(c)-(e), where we zoom in on one particular GB. Figure 3 shows the results of our transport calculations assuming a hydrogen density of 0.35%, which is the amount needed to fully saturate the interior GB sites. The red, blue, and green lines are for hydrogenation of the interior GB sites, the exterior GB sites, and the entire sample, respectively, while the dashed line is for the polycrystalline sample in the absence of hydrogen. In Figure 3(a), there is a clear correlation between the hydrogen distribution and the resulting increase in DOS around zero energy when hydrogen is present outside the interior of the GB, similar to the SW defect. In particular, for a uniform distribution of hydrogen, a resonant peak in the DOS appears near the Dirac point, which is the signature of hydrogenation of pristine graphene. However, when the hydrogenation is confined to the GBs, this peak is strongly suppressed for the exterior sites, and is completely absent for the interior sites. In fact, for interior site hydrogenation

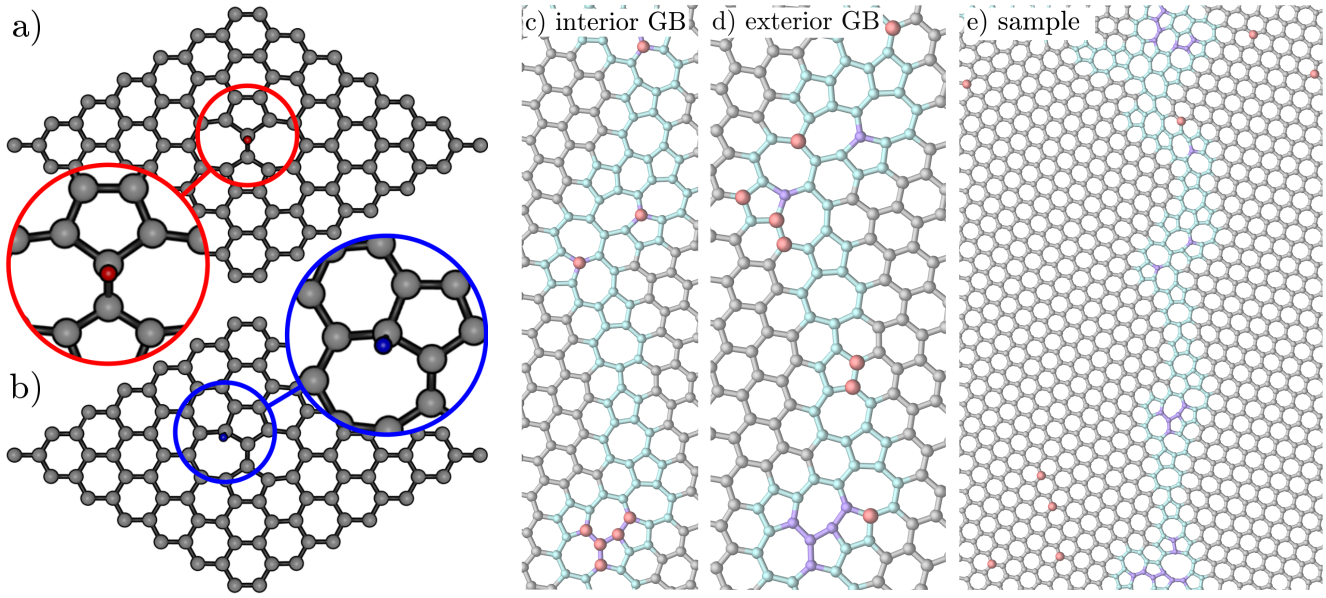

Figure 1: Structural configuration of hydrogen adsorption in defective graphene. Panels (a) and (b) depict adsorption on an interior and exterior site of a Stone-Wales defect, respectively. Panels (c)-(e) show the case of polycrystalline graphene, with adsorption (c) on the interior GB sites, (d) the exterior GB sites, and (e) randomly distributed throughout the sample.

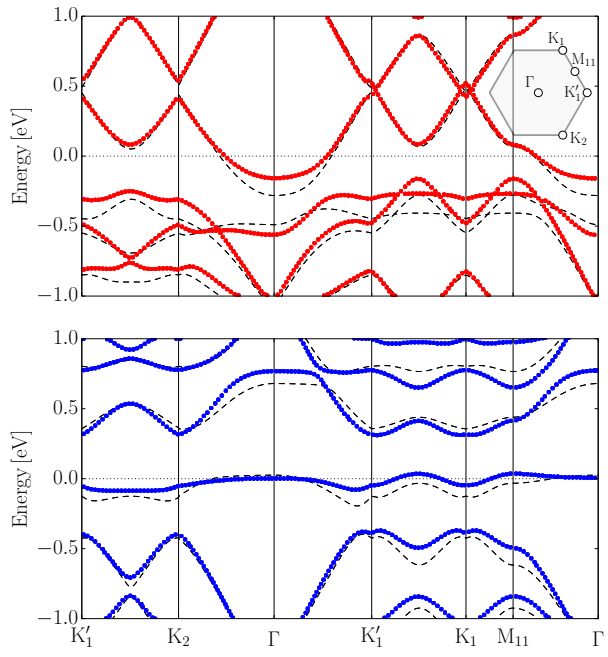

Figure 2: Bandstructure of a hydrogenated Stone-Wales defect. Panel (a) is for adsorption on an interior site, while panel (b) shows the case of adsorption on an exterior defect site. Solid (dashed) lines are obtained from *ab initio* (tight-binding) calculations.

the DOS actually *decreases* on the electron side compared to the polycrystalline sample (polyX) without hydrogen. This behavior is also reflected in the electronic mean free path ℓ_e and the sample mobility μ, shown in Figures 3(b) and (c). Here, uniform hydrogenation significantly reduces ℓ_e and μ, while hydrogenation of the exterior GB sites has a much smaller impact. Meanwhile, hydrogenation of the interior GB sites appears to have, on average, little to no impact on the electrical transport properties of polycrystalline graphene.

In Figure 4 we examine the impact of varying the hydrogen density on the graphene GBs. The solid line is for a hydrogen density of 0.35%, the dotted line is for 0.18%, and the dashed line is for no hydrogen. The main panels of Figure 4 reveal the trends suggested in Figure 3; for the exterior GB sites the mean free path is reduced with an increasing density of hydrogen (Figure 4(b)), while hydrogenation of the interior GB sites has, on average, a negligible impact (Figure 4(a)). However, as noted before, there is an unexpected slight *increase* of the mean free path when hydrogenating the interior GB sites. This behavior is also reflected in the local DOS (LDOS) of the GB atoms, shown in the insets.

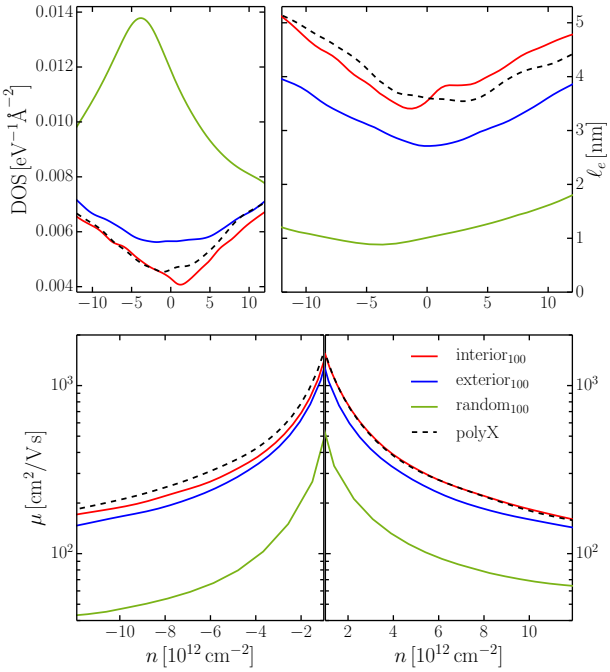

Figure 3: Impact of hydrogen distribution on the electronic (a) density of states, (b) mean free path, and (c) mobility of polycrystalline graphene. The red, blue, and green curves are for hydrogenation on the interior GB sites, exterior GB sites, and a random distribution, respectively, while the dashed line is for the polycrystalline sample without hydrogen. In all cases, the hydrogen defect density is 0.35% corresponding to 100% occupation of the interior GB sites (cf. subscript on labels).

Here one can see that increasing the hydrogenation of the interior GB sites actually decreases the LDOS of the GBs at certain energies. Thus, it appears that hydrogen adsorbates can passivate the defect states associated with graphene GBs, slightly reducing their adverse impact on charge transport. This only appears to be true for the interior GB sites, as the LDOS always increases (and ℓ_e decreases) with increasing hydrogenation of the exterior GB sites.

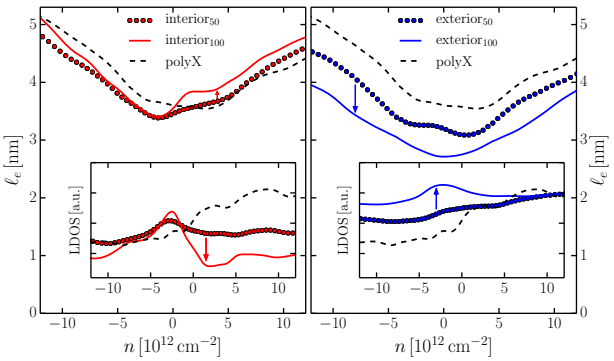

Figure 4: Impact of hydrogen density on the electronic mean free path of polycrystalline graphene. Panel (a) is for hydrogenation of the interior grain boundary sites, while panel (b) is for the exterior grain boundary sites. The solid line is for a hydrogen density of 0.35%, corresponding to full saturation of the interior grain boundary sites. The dotted line is for a hydrogen density of 0.18%, and the dashed curve is for the polycrystalline sample without hydrogenation. The insets show the local density of states, projected over the grain boundary atoms.

Discussion and conclusions

To summarize, we have used *ab initio* and tight-binding calculations to study charge transport in hydrogenated polycrystalline graphene. Our calculations reveal that the zero-energy state usually induced by hydrogen is strongly suppressed or completely absent when the hydrogen sits on a grain boundary. Our calculations also reveal that the presence or absence of this zero-energy defect state have a strong

impact on charge transport through polycrystalline graphene. Earlier work that studied the impact of clusterization of hydrogen on pristine graphene found a similar result – clusterization tended to suppress the formation of the zero-energy state and led to better charge transport in graphene[35]. The dependence on the hydrogen distribution has also important implications for experiments, as recent work showed that depending on the functionalization process, chemical adsorbates can either collect at graphene GBs or they can be distributed throughout the sample[24]. Thus, the exact process of hydrogenation could lead to different results in transport measurements.

Our results can also have important consequences for graphene spintronics. Recent experimental work has shown that the resonant state induced by a hydrogen adsorbate is magnetic, with an exchange splitting of $\sim$20 meV[10]. This local, magnetic resonant state can strongly alter spin relaxation times in graphene[11,12], and is undesirable for the development of graphene-based spintronic devices. The suppression of the resonant state at the GBs suggests that spin lifetimes in polycrystalline graphene may be unaffected by a small density of hydrogen impurities.

Acknowledgement The Center for Nanostructured Graphene (CNG) is sponsored by the Danish National Research Foundation, Project DNRF103. JTF acknowledge support from the Lundbeck foundation (R95-A10510).

References

(1) Novoselov, K. S.; Geim, A. K.; Morozov, S. V.; Jiang, D.; Zhang, Y.; Dubonos, S. V. et al. *Science* **2004**, *306*, 666–669, DOI: 10.1126/science.1102896.

(2) Nair, R. R.; Blake, P.; Grigorenko, A. N.; Novoselov, K. S.; Booth, T. J.; Stauber, T. et al. *Science* **2008**, *320*, 1308–1308, DOI: 10.1126/science.1156965.

(3) Balandin, A. A.; Ghosh, S.; Bao, W.; Calizo, I.; Teweldebrhan, D.; Miao, F. et al. *Nano Letters* **2008**, *8*, 902–907, DOI: 10.1021/nl0731872, PMID: 18284217.

(4) Lee, C.; Wei, X.; Kysar, J. W.; Hone, J. *Science* **2008**, *321*, 385–388, DOI: 10.1126/science.1157996.

(5) Weeks, C.; Hu, J.; Alicea, J.; Franz, M.; Wu, R. *Phys. Rev. X* **2011**, *1*, 021001, DOI: 10.1103/PhysRevX.1.021001.

(6) Zhang, H.; Fonseca, A. F.; Cho, K. *J. Phys. Chem. C* **2014**, *118*, 1436–1442, DOI: 10.1021/jp4096369.

(7) Robinson, J. P.; Schomerus, H.; Oroszlány, L.; Fal'ko, V. I. *Phys. Rev. Lett.* **2008**, *101*, 196803, DOI: 10.1103/PhysRevLett.101.196803.

(8) Wehling, T. O.; Katsnelson, M. I.; Lichtenstein, A. I. *Phys. Rev. B* **2009**, *80*, 085428, DOI: 10.1103/PhysRevB.80.085428.

(9) Jayasingha, R.; Sherehiy, A.; Wu, S.-Y.; Sumanasekera, G. U. *Nano Letters* **2013**, *13*, 5098–5105, DOI: 10.1021/nl402272b.

(10) González-Herrero, H.; Gómez-Rodríguez, J. M.; Mallet, P.; Moaied, M.; Palacios, J. J.; Salgado, C. et al. *Science* **2016**, *352*, 437–441, DOI: 10.1126/science.aad8038.

(11) Kochan, D.; Gmitra, M.; Fabian, J. *Phys. Rev. Lett.* **2014**, *112*, 116602, DOI: 10.1103/PhysRevLett.112.116602.

(12) Kochan, D.; Irmer, S.; Gmitra, M.; Fabian, J. *Phys. Rev. Lett.* **2015**, *115*, 196601, DOI: 10.1103/PhysRevLett.115.196601.

(13) Li, J.; Wang, X.-Y.; Liu, X.-R.; Jin, Z.; Wang, D.; Wan, L.-J. *J. Mater. Chem. C* **2015**, *3*, 3530–3535, DOI: 10.1039/C5TC00235D.

(14) Lin, L.; Li, J.; Ren, H.; Koh, A. L.; Kang, N.; Peng, H. et al. *ACS Nano* **2016**, *10*, 2922–2929, DOI: 10.1021/acsnano.6b00041.

(15) Wu, T.; Zhang, X.; Yuan, Q.; Xue, J.; Lu, G.; Liu, Z. et al. *Nat. Mater.* **2015**, *15*, 43–47, DOI: 10.1038/nmat4477.

(16) Mesaros, A.; Papanikolaou, S.; Flipse, C. F. J.; Sadri, D.; Zaanen, J. *Phys. Rev. B* **2010**, *82*, 205119, DOI: 10.1103/PhysRevB.82.205119.

(17) Huang, P. Y.; Ruiz-Vargas, C. S.; van der Zande, A. M.; Whitney, W. S.; Levendorf, M. P.; Kevek, J. W. et al. *Nature* **2011**, *469*, 389–393, DOI: 10.1038/nature09718.

(18) Kim, K.; Lee, Z.; Regan, W.; Kisielowski, C.; Crommie, M. F.; Zettl, A. *ACS Nano* **2011**, *5*, 2142–2146, DOI: 10.1021/nn1033423.

(19) Yu, Q.; Jauregui, L. A.; Wu, W.; Colby, R.; Tian, J.; Su, Z. et al. *Nat. Mater.* **2011**, *10*, 443–449, DOI: 10.1038/nmat3010.

(20) Tsen, A. W.; Brown, L.; Levendorf, M. P.; Ghahari, F.; Huang, P. Y.; Havener, R. W. et al. *Science* **2012**, *336*, 1143–1146, DOI: 10.1126/science.1218948.

(21) Koepke, J. C.; Wood, J. D.; Estrada, D.; Ong, Z.-Y.; He, K. T.; Pop, E. et al. *ACS Nano* **2013**, *7*, 75–86, DOI: 10.1021/nn302064p.

(22) Salehi-Khojin, A.; Estrada, D.; Lin, K. Y.; Bae, M.-H.; Xiong, F.; Pop, E. et al. *Adv. Mater.* **2012**, *24*, 53–57, DOI: 10.1002/adma.201102663.

(23) Yasaei, P.; Kumar, B.; Hantehzadeh, R.; Kayyalha, M.; Baskin, A.; Repnin, N. et al. *Nat. Commun.* **2014**, *5*, 4911, DOI: 10.1038/ncomms5911.

(24) Seifert, M.; Vargas, J. E. B.; Bobinger, M.; Sachsenhauser, M.; Cummings, A. W.; Roche, S. et al. *2D Materials* **2015**, *2*, 024008.

(25) Boukhvalov, D. W.; Katsnelson, M. I. *Nano Letters* **2008**, *8*, 4373–4379, DOI: 10.1021/nl802234n.

(26) OuYang, F.; Huang, B.; Li, Z.; Xiao, J.; Wang, H.; Xu, H. *The Journal of Physical Chemistry C* **2008**, *112*, 12003–12007, DOI: 10.1021/jp710547x.

(27) Soler, J. M.; Artacho, E.; Gale, J. D.; Garca, A.; Junquera, J.; Ordejn, P. et al. *Journal of Physics: Condensed Matter* **2002**, *14*, 2745.

(28) Perdew, J.; Burke, K.; Ernzerhof, M. *Physical Review Letters* **1996**, *77*, 3865–3868.

(29) Duplock, E. J.; Scheffler, M.; Lindan, P. J. D. *Phys. Rev. Lett.* **2004**, *92*, 225502, DOI: 10.1103/PhysRevLett.92.225502.

(30) Brito, W. H.; Kagimura, R.; Miwa, R. H. *Applied Physics Letters* **2011**, *98*, DOI: http://dx.doi.org/10.1063/1.3592578.

(31) Lieb, E. H. *Phys. Rev. Lett.* **1989**, *62*, 1201–1204, DOI: 10.1103/PhysRevLett.62.1201.

(32) Tuan, D. V.; Kotakoski, J.; Louvet, T.; Ortmann, F.; Meyer, J. C.; Roche, S. *Nano Letters* **2013**, *13*, 1730–1735, DOI: 10.1021/nl400321r.

(33) Roche, S. *Phys. Rev. B* **1999**, *59*, 2284–2291, DOI: 10.1103/PhysRevB.59.2284.

(34) Torres, L. E. F. F.; Roche, S.; Charlier, J.-C. *Introduction to Graphene-Based Nanomaterials*; Cambridge University Press: Cambridge, UK, 2014.

(35) Gargiulo, F.; Autès, G.; Virk, N.; Barthel, S.; Rösner, M.; Toller, L. R. M. et al. *Phys. Rev. Lett.* **2014**, *113*, 246601, DOI: 10.1103/PhysRevLett.113.246601.